Chinese Chemical Letters 33 (2022) 4695–4699

Contents lists available at ScienceDirect

Chinese Chemical Letters

journal homepage: www.elsevier.com/locate/cclet

Inherently hydrophilic mesoporous channel coupled with metal oxide for fishing endogenous salivary glycopeptides and phosphopeptides

Zixing Xu[a], Yonglei Wu[a], Xufang Hu[c,*], Chunhui Deng[a,b,*], Nianrong Sun[b,*]

[a] Department of Chemistry, Fudan University, Shanghai 200433, China
[b] Department of Gastroenterology and Hepatology, Zhongshan Hospital, Fudan University, Shanghai 200032, China
[c] School of Chemical Science and Technology, Yunnan University, Kunming 650091, China

ARTICLE INFO

Article history:
Received 11 October 2021
Revised 5 November 2021
Accepted 23 December 2021
Available online 29 December 2021

Keywords:
Mesoporous material
Hydrophilic interaction liquid chromatography
Metal oxide affinity chromatography
Human saliva
Endogenous phosphopeptides
Endogenous glycopeptides

ABSTRACT

Both glycosylation and phosphorylation exert crucial rule in multitudinous biological processes. For in-depth profiling of glycosylation and phosphorylation, a magnetic metal oxide is effectively coupled with inherently hydrophilic mesoporous channels (denoted as Fe_3O_4@TiO_2@mSiO_2-TSG). Based on the mechanism of hydrophilic interaction liquid chromatography (HILIC) and metal oxide affinity chromatography (MOAC), the Fe_3O_4@TiO_2@mSiO_2-TSG nanomaterial shows high capacity for simultaneously enriching glycopeptides and phosphopeptides. With human saliva collected in successive four days as practical biological sample, endogenous glycopeptides and phosphopeptides are efficiently enriched. Further gene ontology analysis reveals that the identified endogenous glycopeptides and phosphopeptides participate in diverse molecular functions and biological processes. This strategy is anticipated to promote variation analysis of salivary post-translational modifications.

Glycosylation and phosphorylation are two crucial protein processing modes and protein post-translational modifications (PTMs) [1], which exert significant impacts on regulating cell differentiation and proliferation [2], intracellular communication [3], immune response [4], and transcriptional activation [5]. Numerous reports have revealed glycosylation and phosphorylation not only independently perform their own duties but also cooperatively regulate diverse biologic and pathogenic processes [6–8]. For instance, the glycosylation and phosphorylation of tau protein and β-amyloid precursor protein are considered to modulate Alzheimer's disease *via* accumulation and aggregation [9,10]. Endogenous glycopeptides and phosphopeptides, as important products of the two PTMs, are sensitive biomarkers for the prediction, diagnosis, and monitoring of many diseases [11,12]. Serum glycopeptidome can be used to assess the risk of hepatitis B virus-related liver diseases [13]. Major histocompatibility complex class I-associated phosphopeptides are thought to be the hallmarks of malignant transformation [14]. Therefore, integrative analysis of endogenous glycopeptides and phosphopeptides is anticipated to promote the discovery of biomarker and increase knowledge of the two PTMs mechanisms.

Mass spectrometry (MS) technique with high speed, high throughput and high sensitivity has become a prevalent and reliable tool for varied research fields especially in proteomics [15]. However, direct analysis of endogenous glycopeptides and phosphopeptides is often hindered by their low abundance and ionization, and especially complex interferences. Therefore, many strategies have been developed for the enrichment of glycopeptides and phosphopeptides. Among them, hydrophilic interaction liquid chromatography (HILIC) and metal oxide affinity chromatography (MOAC) are common strategies. The former provides unbiased binding to glycopeptides and the latter possesses pH-controlled strong affinity to phosphopeptides [16–18]. Thus, the combination of HILIC and MOAC has been considered as a great idea for the simultaneous enrichment of glycopeptides and phosphopeptides. Lu *et al.* proposed the PNI-co-$ATBA_{0.2}$@SiO_2 material and identified 631 phosphopeptides and 120 glycopeptides from 50 μg HeLa cell lysates [19]. Sun *et al.* designed a hydrophilic iminodiacetic acid-modified magnetic titanium dioxide and simultaneously enriched 550 phosphopeptides and 330 glycopeptides from tryptic digestion of 100 μg mouse brain extracts [20]. However, there are few reports regarding the simultaneous analysis of endogenous glycopeptidome and phosphopeptidome due to the high dynamic range of body fluid and the trace amounts of endogenous glycopeptides and phosphopeptides, making it a very challenging task. Therefore, it is encouraging to explore novel functionalized material to resolve this challenge.

* Corresponding authors.
E-mail addresses: huxufang@yun.edu.cn (X. Hu), chdeng@fudan.edu.cn (C. Deng), sunnianrong@fudan.edu.cn (N. Sun).

https://doi.org/10.1016/j.cclet.2021.12.069
1001-8417/

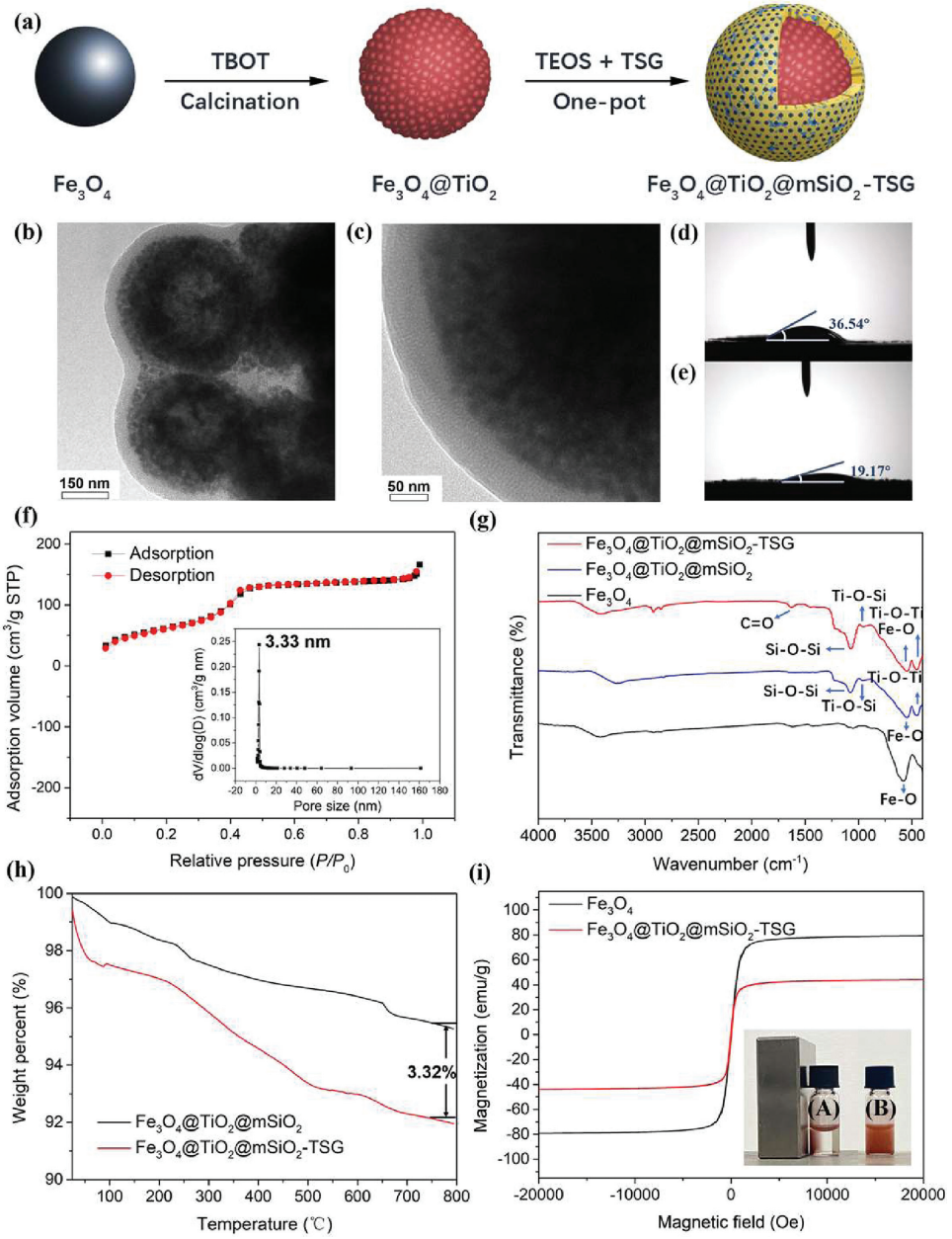

Fig 1. (a) Synthesis flow chart of Fe_3O_4@TiO_2@mSiO_2-TSG; (b, c) TEM images of Fe_3O_4@TiO_2@mSiO_2-TSG; water contact angles of (d) Fe_3O_4@TiO_2@mSiO_2 and (e) Fe_3O_4@TiO_2@mSiO_2-TSG. (f) Nitrogen adsorption-desorption isotherms and pore size distribution curve of Fe_3O_4@TiO_2@mSiO_2-TSG. (g) FT-IR spectra of Fe_3O_4, Fe_3O_4@TiO_2@mSiO_2, Fe_3O_4@TiO_2@mSiO_2-TSG. (h) TGA curves of Fe_3O_4@TiO_2@mSiO_2 and Fe_3O_4@TiO_2@mSiO_2-TSG. (i) Magnetic hysteresis curves of Fe_3O_4 and Fe_3O_4@TiO_2@mSiO_2-TSG, the inset in (i) shows (A) the magnetic separation and (B) dispersion processes of the Fe_3O_4@TiO_2@mSiO_2-TSG.

In this work, we constructed a magnetic metal oxide nanocomposite coupled with inherently hydrophilic mesoporous channels (denoted as Fe_3O_4@TiO_2@mSiO_2-TSG). The Fe_3O_4 core undertook the self-assembly of TiO_2 layer, and hydrophilic mesoporous silica layer containing abundant gluconamide was further modified onto TiO_2 layer *via* a facile one-pot method. Generally, superparamagnetism of innermost Fe_3O_4 core allowed rapid sample separation. The middle TiO_2 layer could chelate with phosphoryl oxygens of phosphopeptides [21]. The outermost hydrophilic mesoporous silica layer not only provided intense hydrophilic attraction for glycopeptides [22], but also provided large specific surface area for accommodating glyco-/phosphopeptides and restrained large-sized proteins from entering into the perpendicular mesochannels [23,24]. Based on above features, Fe_3O_4@TiO_2@mSiO_2-TSG revealed satisfactory co-enrichment efficiency in both standard samples and complex saliva samples. It is noteworthy that our material intelligently integrates HILIC and MOAC with a comparatively convenient manner for endogenous glycopeptidomics and phosphopeptidomics research.

The synthesis approach of Fe_3O_4@TiO_2@mSiO_2-TSG is illustrated in Fig. 1a. Briefly, the Fe_3O_4 sphere was firstly synthesized *via* a renowned solvothermal approach [25]. Fe_3O_4@TiO_2 was obtained by the hydrolysis and condensation of titania precursor (tetrabutyl titanate) on the magnetic nanoparticles. Subsequently, hydrophilic silica layer was coated on TiO_2 shell through a facile one-pot sol-gel spontaneous growth method, for which tetraethyl orthosilicate (TEOS) and *N*-(3-triethoxysilylpropyl)gluconamide (TSG) were adopted as silica source, and cetyltrimethylammonium bromide (CTAB) served as surfactant template. Finally, after refluxing to remove CTAB, Fe_3O_4@TiO_2@mSiO_2-TSG nanomaterial

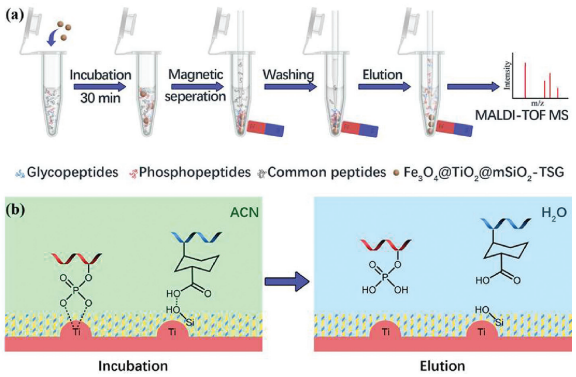

Fig 2. (a) Workflow chart of Fe_3O_4@TiO_2@$mSiO_2$-TSG for glycopeptide enrichment from biological samples; (b) binding modes between glycopeptides/phosphopeptides and functional groups of Fe_3O_4@TiO_2@$mSiO_2$-TSG in different conditions.

was obtained. Transmission electron microscope (TEM) images of Fe_3O_4@TiO_2@$mSiO_2$-TSG illustrate the core-shell structure and perpendicularly aligned mesoporous channels (Figs. 1b and c). The hydrophilicity was evaluated through measuring the water contact angle of Fe_3O_4@TiO_2@$mSiO_2$ and Fe_3O_4@TiO_2@$mSiO_2$-TSG (Figs. 1d and e). The obvious decrease from 36.54° to 19.17° confirms that the introduction of gluconamide considerably enhance the material hydrophilicity. The nitrogen adsorption-desorption measurements of Fe_3O_4@TiO_2@$mSiO_2$-TSG indicate the surface area is around 229.7 m^2/g and the pore size is about 3.33 nm (Fig. 1f), which endows the material with size-exclusion effect. Scanning electron microscope (SEM) images with the corresponding EDX elemental mapping images (Figs. S1 and S2 in Supporting information) distinctly display that C, N, O, Fe and Si elements are homogeneously distributed, implying the successful modification of TiO_2 and gluconamide functionalized silica layer. Moreover, Fourier-transform infrared spectroscopy (FT-IR) analysis of different materials is displayed in Fig. 1g. The absorption peaks at 450–700 cm^{-1} are ascribed to Ti−O−Ti, at 1640 cm^{-1}, 1080 cm^{-1}, 910 cm^{-1} and 582 cm^{-1} belonged to C=O, Si−O−Si, Ti−O−Si and Fe−O, respectively. Thermo-gravimetric analysis (TGA, Fig. 1h) shows weight loss between Fe_3O_4@TiO_2@$mSiO_2$-TSG and Fe_3O_4@TiO_2@$mSiO_2$ is about 3.32%, revealing the high content of gluconamide moiety. Besides, the saturation magnetic (Ms) values of Fe_3O_4 and Fe_3O_4@TiO_2@$mSiO_2$-TSG are measured as 79.15 emu/g and 44.12 emu/g, respectively (Fig. 1i), and as shown in inset of Fig. 1i, the uniformly dispersed Fe_3O_4@TiO_2@$mSiO_2$-TSG in solution could be separated sufficiently with the aid of a magnet, demonstrating the Ms value of Fe_3O_4@TiO_2@$mSiO_2$-TSG is sufficient for high-efficient magnetic separation.

The enrichment procedure for glycopeptides and phosphopeptides by Fe_3O_4@TiO_2@$mSiO_2$-TSG mainly includes incubation, washing, elution and MS analysis (Fig. 2a). The potential binding modes between Fe_3O_4@TiO_2@$mSiO_2$-TSG and glyco- and phosphopeptides are briefly manifested in Fig. 2b. In enrichment condition, TiO_2 can coordinate with phosphate groups on the phosphopeptides [26], the hydroxyl groups on $mSiO_2$-TSG and glycopeptides could form an intricate network of hydrogen bonding and electrostatic interaction. While in eluting condition, the interaction can be broken, thus realizing the enrichment of glyco- and phosphopeptides. The enrichment performance of Fe_3O_4@TiO_2@$mSiO_2$-TSG was first investigated by capturing glycopeptides from 100 nmol/L horseradish peroxidase (HRP) tryptic digests. Herein, under optimized condition (Fig. S3 in Supporting information), HRP digests, β-casein digests and Fe_3O_4@TiO_2@$mSiO_2$-TSG were respectively dispersed in loading buffer. After incubation, washing and elution, the eluent was analyzed by MALDI-TOF MS. Detailed information of enrichment procedure could be found in the Supporting information. As shown in Figs. 3a and b, the intensity of glycopeptides is extremely low as a result of suffering from interferences when conducting direct analysis. While after enrichment, 8 glycopeptides and 10 glycopeptide fragments dominate the spectrum, the detailed information of the identified glycopeptides is listed at Table S1 (Supporting information). Besides, 100 nmol/L tryptic digests of human immunoglobulin G (IgG) were also applied, as shown in Figs. 3c and d, impurity peaks are removed, 5 glycopeptides and 14 glycopeptide fragments could be clearly observed after enrichment, the detailed information of the identified glycopeptides is listed in Table S2 (Supporting information). The phosphopeptide enrichment capacity of Fe_3O_4@TiO_2@$mSiO_2$-TSG was evaluated by 100 nmol/L β-casein tryptic digests (containing 2% α-casein), as shown in Figs. 3e and f, 6 phosphopeptide peaks and 10 fragment peaks are distinctly detected, the detailed information of the identified phosphopeptides is listed in Table S3 (Supporting information). Furthermore, when using the mixture of 100 nmol/L HRP tryptic digests and β-casein tryptic digests as sample (Figs. 3g and h), after enrichment, the spectrum is occupied by 8 glycopeptide peaks and 6 phosphopeptide peaks, as well as their corresponding 15 fragment peaks. It can be seen the number of the detected glycopeptides and phosphopeptides by co-enrichment is consistent with that of respective enrichment. While the production of fragment peaks is associated with the ionization degree of the analytes, the matrix effect caused by ion suppression affects the ionization of co-eluting analytes, influencing the precision and accuracy of fragment peaks [27]. This result indicates our method is great in co-enrichment.

The reusability of Fe_3O_4@TiO_2@$mSiO_2$-TSG for simultaneous enrichment was investigated, the nanomaterial was recycled by washing with loading buffer and eluents. Even when the regenerated Fe_3O_4@TiO_2@$mSiO_2$-TSG was reused for six enrichment experiments, the number of identified peptides and relative intensity are nearly identical to that obtained for the first use (Fig. S4 in Supporting information), which confirms the reusability of the Fe_3O_4@TiO_2@$mSiO_2$-TSG. Furthermore, the concentration of HRP digests and β-casein digests were diluted to 1 nmol/L and 0.1 nmol/L, as shown in Fig. S5 (Supporting information), glyco- and phosphopeptide peaks still occupy the spectra after enrichment by Fe_3O_4@TiO_2@$mSiO_2$-TSG, indicating the excellent sensitivity for co-enrichment.

The selectivity of Fe_3O_4@TiO_2@$mSiO_2$-TSG for glyco- and phosphopeptide enrichment was tested as well. HRP or β-casein tryptic digests were mixed respectively with BSA tryptic digests. When molar ratio reaches 1:200, the signals of glyocopeptide or phosphopeptide peaks are significantly suppressed. However, glycopeptide peaks and phosphopeptide peaks take a predominant position in the spectrum after enrichment with Fe_3O_4@TiO_2@$mSiO_2$-TSG (Fig. S6 in Supporting information). Furthermore, considering the numerous variables with regard to the composition of complex biological samples, the size-exclusion effect of Fe_3O_4@TiO_2@$mSiO_2$-TSG nanomaterial was assessed (Fig. S7 in Supporting information). HRP tryptic digests and β-casein tryptic digests were mixed with bovine albumin protein respectively with the ratio of 1:5000 (w/w). The signals of glycopeptide and phosphopeptide are suppressed significantly and BSA protein peaks could be detected before enrichment. While after enrichment, the peaks of glycopeptides and phosphopeptides occupy the spectrum and no BSA protein peak could be detected. The comparisons indicate the remarkable size-exclusion property of Fe_3O_4@TiO_2@$mSiO_2$-TSG.

Inspired by the excellent enrichment performance above, the Fe_3O_4@TiO_2@$mSiO_2$-TSG nanocomposites were applied to the enrichment of glycopeptides and phosphopeptides from non-digested human saliva within four days in succession, the eluent was desalted by SepPak C18 cartridges, deglycosylated by PNGaseF and

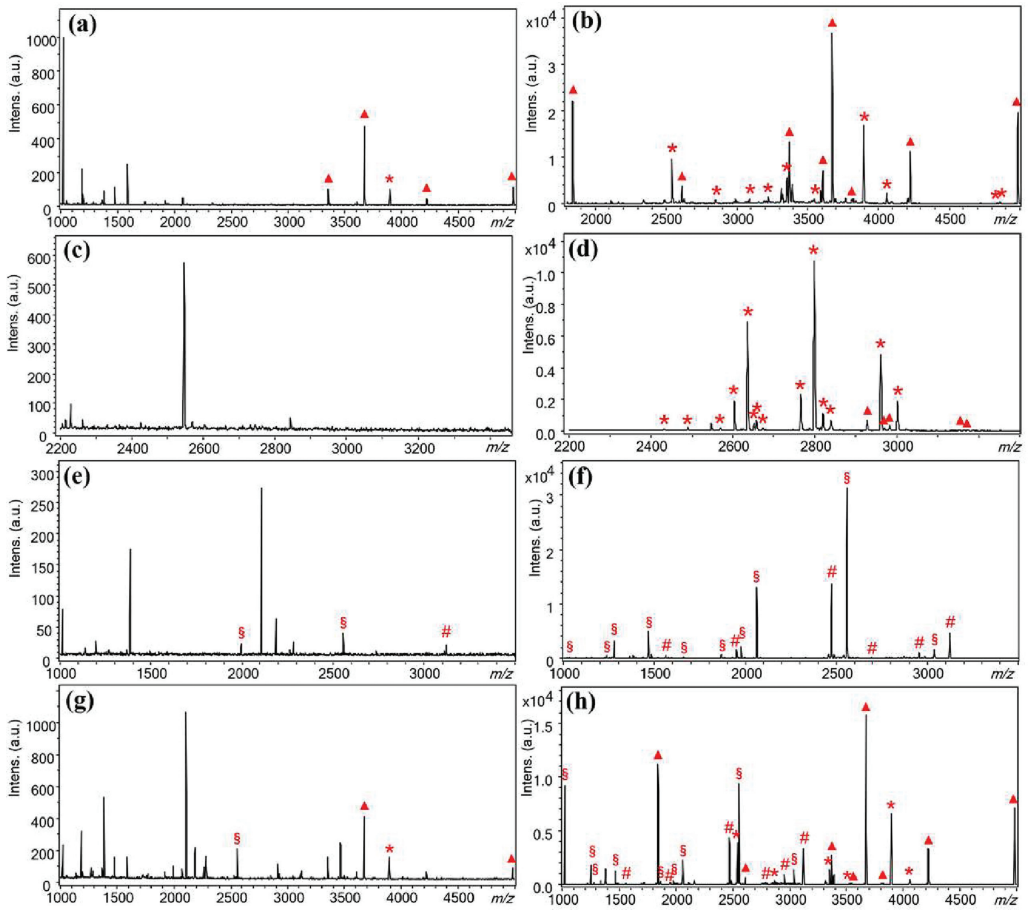

Fig 3. MALDI-TOF MS spectra of 100 nmol/L tryptic digests of (a, b) HRP, (c, d) IgG, and (e, f) β-casein, as well as (g, h) mixed HRP and β-casein. (a, c, e, g) direct analysis; (b, d, f, h) after enrichment by Fe_3O_4@TiO_2@$mSiO_2$-TSG. "△", glycopeptides; "*", glycopeptide fragments; "#", phosphopeptides; "§", phosphopeptide fragments.

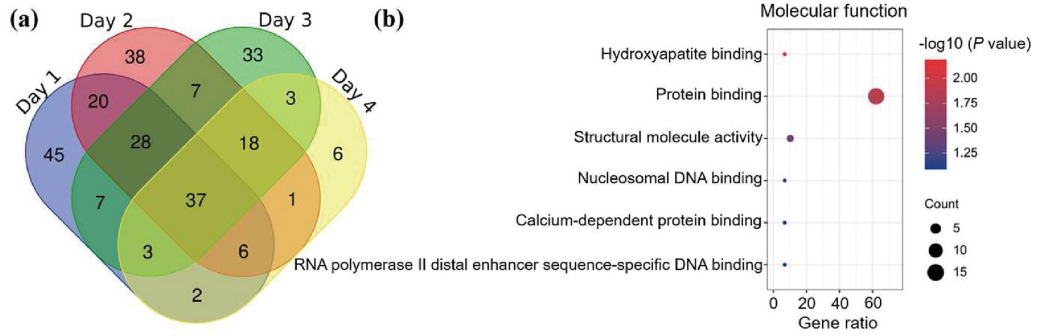

Fig 4. (a) Venn diagram of the identified glycopeptides and phosphopeptides of the healthy volunteer in four days; (b) the gene ontology (GO) term enrichment analysis of the molecular function of the healthy volunteer.

lyophilized for nano-LC-MS/MS analysis. 31, 63, 53, 39 glycopeptides and 132, 105, 87, 39 phosphopeptides were identified in four days, the selectivity reached 12.2%. The detailed information is listed in Tables S4 and S5 (Supporting information). As shown in Fig. 4a and Fig. S8 (Supporting information), a total of 94 endogenous glycopeptides and 164 endogenous phosphopeptides are enriched from a total of 2 μL human saliva. A brief comparison concerning reported strategies for endogenous glycopeptide and phosphopeptide enrichment in human saliva is listed in Table S6 (Supporting information) [28–44]. The comparison of these methods manifests that the Fe_3O_4@TiO_2@$mSiO_2$-TSG nanomaterial possesses competitive efficiency in endogenous glyco- and phosphopeptide enrichment. Moreover, the gene ontology analysis was conducted. The salivary glyco- and phosphopeptides are inclined to localize at extracellular region, extracellular exosome and extracellular space (Fig. S9 in Supporting information). As shown in Fig. 4b, the salivary glyco- and phosphopeptides play crucial roles in protein binding and DNA binding. Besides, the identified endogenous peptides derived from basic salivary proline-rich protein tend to undergo both phosphorylation and glycosylation, as shown in Fig. S10 (Supporting information), they are associated with a series of biological processes including induction of bacterial agglutination, platelet degranulation and defense response to bacterium, which contribute to the anti-bacteria property of saliva.

In summary, a facile synthesis method of constructing a novel hydrophilic magnetic titanium dioxide mesoporous silica mate-

rial for glycopeptidomics and phosphopeptidomics analysis was proposed. TiO_2 was deposited facilely on the magnetic sphere, and the gluconamide-functionalized mesoporous silica was synthesized *via* one-pot synthetic approach, which significantly simplify the synthetic method compared to conventional hydrophilic material based on post-synthetic functionalization. Owing to the enhanced hydrophilicity, abundant metal oxide site, suitable mesoporous structure, large specific surface area and considerable magnetic responsiveness, Fe_3O_4@TiO_2@mSiO_2-TSG exhibited outstanding sensitivity, reusability and size-exclusion effect towards glycophopeptide and phosphopeptide enrichment. Remarkably, a total of 94 endogenous glycopeptides and 164 endogenous phosphopeptides were captured from a total of 2 μL non-digested human saliva with the aid of Fe_3O_4@TiO_2@mSiO_2-TSG. Gene ontology analysis revealed the identified salivary glyco- and phosphopeptides exert influence on diverse biological processes. The high simultaneous enrichment capacity makes the Fe_3O_4@TiO_2@mSiO_2-TSG a potent tool for glycoproteomics and phosphoproteomics analysis and suggests a huge potential in comprehensive post-translational modifications research.

Declaration of competing interest

The authors declare no conflict of interest.

Acknowledgments

This work was supported by National Key R&D Program of China (No. 2018YFA0507501), the National Science Foundation for Distinguished Young Scholars of China (No. 21425518), the National Natural Science Foundation of China (Nos. 22074019, 22004017), and Shanghai Sailing Program (No. 20YF1405300).

References

[1] Y. Li, X.M. Zhang, C.H. Deng, Chem. Soc. Rev. 42 (2013) 8517–8539.
[2] G.Y. Qing, Q. Lu, Y.T. Xiong, et al., Adv. Mater. 29 (2017) 1604670.
[3] C.W. Li, S.O. Lim, W.Y. Xia, et al., Nat. Commun. 7 (2016) 12632.
[4] H.Y. Zheng, S. Guan, X.T. Wang, et al., Anal. Chem. 92 (2020) 9239–9246.
[5] G.Y. Qing, Q. Lu, X.L. Li, et al., Nat. Commun. 8 (2017) 461.
[6] C.M. Woo, A.T. Iavarone, D.R. Spiciarich, K.K. Palaniappan, C.R. Bertozzi, Nat. Methods 12 (2015) 561–567.
[7] X.J. Zou, J.Z. Jie, B. Yang, Anal. Chem. 89 (2017) 7520–7526.
[8] H.J. Zheng, J.X. Jia, Z. Li, Q. Jia, Anal. Chem. 92 (2020) 2680–2689.
[9] A.J. Maetorell, A.L. Paulson, H.J. Suk, et al., Cell 177 (2019) 256–271.
[10] E.F. Fang, Y. Hou, K. Palikaras, et al., Nat. Neurosci. 22 (2019) 401–412.
[11] T.J. Wadzinski, A. Steinauer, L. Hie, et al., Nat. Chem. 10 (2018) 644–652.
[12] Q.J. Liu, N.R. Sun, M.X. Gao, et al., ACS Sustain. Chem. Eng. 6 (2018) 4382–4389.
[13] S. Zhang, X.Y. Cao, C. Liu, et al., Mol. Cell. Proteom. 18 (2019) 2262–2272.
[14] F. Mohammed, M. Cobbold, A.L. Zarling, et al., Nat. Immunol. 9 (2008) 1236–1243.
[15] R. Aebersold, M. Mann, Nature 537 (2016) 347–355.
[16] Y. Li, N.R. Sun, X.F. Hu, Y. Li, C.H. Deng, TrAC Trends Anal. Chem. 120 (2019) 115658.
[17] N.R. Sun, H. Wu, H.M. Chen, X.Z. Shen, C.H. Deng, Chem. Commun. 55 (2019) 10359–10375.
[18] N.R. Sun, H. Wu, X.Z. Shen, C.H. Deng, Adv. Funct. Mater. 29 (2019) 1900253.
[19] Q. Lu, C. Chen, Y.T. Xiong, et al., Anal. Chem. 92 (2020) 6269–6277.
[20] N.R. Sun, H. Wu, X.Z. Shen, Microchim. Acta 187 (2020) 195.
[21] H.J. Zhou, M.L. Ye, J. Dong, et al., Nat. Protoc. 8 (2013) 461–480.
[22] D.V. McCalley, J. Chromatogr. A 1523 (2017) 49–71.
[23] C.L. Pu, H.L. Zhao, Y.Y. Hong, et al., ACS Sustain. Chem. Eng. 9 (2021) 5818–5826.
[24] Y.L. Li, H. Wu, N.R. Sun, C.H. Deng, J. Chromatogr. A 1587 (2019) 24–33.
[25] T.C. Zhao, X.H. Zhu, C.T. Hung, et al., J. Am. Chem. Soc. 140 (2018) 10009–10015.
[26] G.L. Barbera, A.L. Capriotti, C. Cavaliere, et al., Talanta 183 (2018) 245–249.
[27] S. Alseekh, A. Aharoni, Y. Brotman, et al., Nat. Methods 18 (2021) 747–756.
[28] Y.L. Li, C.H. Deng, N.R. Sun, Anal. Chim. Acta 1024 (2018) 84–92.
[29] C. Zhang, X.D. Jin, L.P. Wang, et al., ACS Appl. Mater. Interfaces 13 (2021) 9714–9728.
[30] H.M. Chen, Y.L. Li, H. Wu, N.R. Sun, C.H. Deng, ACS Sustain. Chem. Eng. 7 (2019) 2844–2851.
[31] Y.L. Li, H. Wu, N.R. Sun, C.H. Deng, J. Chromatogr. A 1587 (2019) 24–33.
[32] N.R. Sun, J.W. Wang, J.Z. Yao, H.M. Chen, C.H. Deng, Microchim. Acta 186 (2019) 159.
[33] Z.D. Wang, R.Q. Wu, H.M. Chen, N.R. Sun, C.H. Deng, Nanoscale 10 (2018) 5335–5341.
[34] X.W. Li, H.Y. Zhang, N. Zhang, et al., ACS Sustain. Chem. Eng. 7 (2019) 11511–11520.
[35] Y. Tian, R. Tang, X. Wang, et al., Anal. Chim. Acta 1173 (2021) 338694.
[36] L.H. Yi, Y.H. Yan, K.Q. Tang, C.F. Ding, Anal. Methods 12 (2020) 4657–4664.
[37] B. Liu, B.C. Wang, Y.H. Yan, K.Q. Tang, C.F. Ding, Microchim. Acta 188 (2021) 1–11.
[38] Y.L. Li, L.L. Liu, H. Wu, C.H. Deng, Anal. Chim. Acta 1079 (2019) 111–119.
[39] Z.X. Xu, Y.L. Wu, H. Wu, N.R. Sun, C.H. Deng, Anal. Chim. Acta 1146 (2021) 53–60.
[40] D.P. Xu, G.Q. Yan, M.X. Gao, C.H. Deng, X.M. Zhang, Talanta 166 (2017) 154–161.
[41] Y.L. Wu, Q.J. Liu, Y.Q. Xie, C.H. Deng, Talanta 190 (2018) 298–312.
[42] M.M. Ali, Z.Y. Zhu, D. Hussain, et al., Talanta 233 (2021) 122576.
[43] H.Z. Lin, K.P. Yuan, C.H. Deng, Talanta 175 (2017) 427–434.
[44] R.Z. Tang, Y. Yu, J. Dong, et al., Anal. Chim. Acta 1144 (2021) 111–120.